Received: 3 May 2023 | Revised: 8 September 2023 | Accepted: 25 September 2023

DOI: 10.1002/mawe.202300007

ARTICLE

WILEY VCH

# Influence of cryogenic turning strategies on the surface morphology and resulting wear behavior of metastable AISI 347 austenitic stainless steel

## Einfluss von kryogenen Drehstrategien auf die Oberflächenmorphologie und das resultierende Verschleißverhalten des metastabilen austenitischen rostfreien Stahls X6CrNiNb18-10

**T. Zhu**[1] | **M. Smaga**[1] | **S. Thielen**[2] | **H. Hotz**[3] | **B. Kirsch**[3] | **J. C. Aurich**[3] | **B. Sauer**[2] | **O. Koch**[2] | **T. Beck**[1]

[1]University of Kaiserslautern-Landau, Institute of Materials Science and Engineering, Kaiserslautern, Germany

[2]University of Kaiserslautern-Landau, Institute of Machine Elements, Gears, & Transmissions, Kaiserslautern, Germany

[3]University of Kaiserslautern-Landau, Institute for Manufacturing Technology and Production Systems, Kaiserslautern, Germany

**Correspondence**
M. Smaga, University of Kaiserslautern-Landau, Institute of Materials Science and Engineering, Gottlieb-Daimler-Straße 44, 67663 Kaiserslautern, Germany.
Email: m.smaga@mv.rptu.de

**Funding information**
Deutsche Forschungsgemeinschaft (DFG, German Research Foundation), Grant/Award Number: 172116086 – SFB 926

**Abstract**

Cryogenic turning of metastable austenitic stainless steels can improve wear resistance of the resulting surface due to the phase transformation of γ-austenite into α'- and/or ε-martensite in the near surface layer. By using a cryogenic two-step turning process, the amount of deformation-induced α'-martensite in the subsurface regime can be further increased. To determine the influence of the implemented and optimized two-step turning strategy on the tribological properties of countersurfaces for radial shaft seals, an evaluation of wear behavior of the shaft seal countersurface as well as microstructural analyses in subsurface regime is presented and compared to the cryogenic single step turning process. The results show that not only the integral phase transformation in the overall subsurface region, but also the local phase distribution plays an important role when it comes to the surface performance in tribological applications.

**KEYWORDS**
cryogenic turning, deformation induced martensite, metastable austenite, radial shaft seal, wear resistance

**Abstract**

Das kryogene Drehen von metastabilen austenitischen rostfreien Stählen kann die Verschleißfestigkeit der resultierenden Oberfläche aufgrund der Phasenumwandlung von γ-Austenit nach α'- und/oder ε-Martensit im

oberflächennahen Bereich verbessern. Durch den Einsatz eines zweistufigen kryogenen Drehprozesses kann der verformungsinduzierte α'-Martensitgehalt weiter erhöht werden. Um den Einfluss des implementierten und optimierten zweistufigen kryogenen Drehprozesses auf die tribologischen Eigenschaften von Gegenlaufflächen für Radialwellendichtringe zu ermitteln, werden die Verschleißuntersuchungen der Wellendichtring-Gegenlauffläche sowie die Mikrostrukturanalysen in den oberflächennahen Bereichen durchgeführt und mit der einstufigen Drehstrategie verglichen. Die Ergebnisse zeigen, dass nicht nur die integrale Phasenumwandlung in der gesamten Einflusszone, sondern auch die lokale Phasenverteilung eine wichtige Rolle für die Oberflächenqualität in tribologischen Anwendungen spielen.

**SCHLÜSSELWÖRTER**
kryogenes Drehen, metastabiler Austenit, Radialdichtwelle, verformungsinduzierter Martensit, Verschleißbeständigkeit

## 1 | INTRODUCTION

Surface hardness and wear resistance play important roles in many engineering applications where two bodies are in contact, for example: shaft counterfaces of radial shaft seals which are exposed to high tribological loads [1]. Usually both properties are modified in a dedicated process before or after the manufacturing of the part's final shape, like coating or surface hardening. A high hardness in the surface layer is required to prevent excessive wear and to guarantee their functionality [2]. A combination of the hardening and shaping process in one step would enable a significant reduction in production cost and time.

Deformation-induced phase transformation from γ-austenite into α'- and/or ε-martensite can be achieved in metastable austenitic steels if thermal and mechanical loads are chosen appropriately, which improves the material strength and resulting wear resistance as well as fatigue behavior [1, 3, 4]. Regarding the manufacturing process, thermomechanical loads can be specifically controlled by varying machining parameters, such as cutting speed, depth of cut, tool properties and cooling strategy. Thus, the surface layer properties, respectively the mechanical functionality of the workpiece, can be influenced. From this perspective, the process optimization which leads to advantageous surface layer properties has a high economic significance. In addition, cryogenic cooling media such as carbon dioxide or liquid nitrogen are often used to improve surface layer properties [5]. For various materials, an increase in hardness was observed in the workpiece surface layer after cryogenic machining, which results from strain hardening mechanisms like grain refinement, twinning and the increase of dislocation density, as well as compressive residual stresses [6–8]. By cryogenic turning of metastable austenitic steels, the phase transformation from γ-austenite to α'- and ε-martensite in the workpiece surface layer was reported to superimpose the above-mentioned hardening mechanisms [9]. A previous study has shown that shaft counterfaces produced in this way achieve better wear-resistance than the state-of-the-art ground components made of hardened steel [1].

## 2 | STATE OF THE ART

### 2.1 | Manufacturing of seal counterfaces

Since the kinematics of the turning process cause macro-twist on the surface and thereby a pumping effect in the sealing contact during shaft rotation, for many years turned shafts have only been used in applications with fixed rotational direction [1]. Previous studies have shown that surfaces turned with a conventional turning process can be leak-tight in both rotational directions despite the presence of the twist if appropriate manufacturing parameters are chosen [1, 10]. Different turning processes have been investigated by several researchers and results show that turning can produce functional sealing counterfaces, e.g., a hard-turning process which enables the turning of twist free surfaces using a special kinematic of the tool [11–14]. For applications with low lifetime requirements, such as the soft-turned counterfaces of 42CrMo4 shafts, tangential turning and grooving were applied instead of grinding to reduce manufacturing costs [15]. Moreover, a two-step turning process with reciprocal feed direction was investigated by the authors'

team, where the twist generated by each turning step is supposed to be eliminated. The study showed that leak-tight counterfaces can be manufactured with appropriate turning parameters [16]. Some seal manufacturers also give recommendations for turned surfaces [17].

## 2.2 | Wear of seal counterfaces

Since the sealing edge is usually molded, it is covered by a smooth molding skin in new condition. During the run-in process, this skin is worn off, exposing filler particles in the bulk material, Figure 1 [18]. In order to ensure the formation of a rough sealing edge, which is necessary for the reverse pumping effect during this wear process, special rubber compounds containing coarse filler particles made from inorganic materials such as quartz, chalk or other mineral fillers are used [19–21]. Especially the quartz particles are able to cause wear on the shaft surface, since their hardness (750 HV 10–1150 HV 10) exceeds the typical hardness of state of the art counterfaces in such applications (600 HV 10) [20].

## 2.3 | Metastable austenite

Metastable austenitic stainless steels can undergo phase transformation due to plastic deformation. Hence, the face-centered cubic (fcc) γ-austenitic lattice structure can be transformed into body-centered cubic (bcc) α'-martensite and/or hexagonal-close-packed (hcp) ε-martensite, which are thermodynamically more stable than the original austenitic structure at ambient temperature [22]. Based on the chemical composition, the stability of the austenitic structure can be roughly estimated with the empirical equation of $M_{d30}$-temperature, at which 50 % of initial austenite transforms to α'-martensite due to a true tensile strain of 30 %. Similarly, the martensite start temperature ($M_s$) as well as the stacking fault energy (SFE) are also widely used as a criterion for the austenite stability in the literature [23–25]. Besides the chemical composition, the austenite stability can also be strongly influenced by the temperature, grain size, strain rate, deformation mode, etc. [4]. Previous studies have shown a clear improvement of mechanical properties like fatigue behavior and wear resistance by proper implementations of the above-mentioned microstructural changes [1, 3].

# 3 | INVESTIGATED MATERIAL

The metastable austenitic stainless steel AISI 347 (1.4550, X6CrNiNb1810) was used in this study. The chemical composition of test material was investigated using spectral analysis, which was used to calculate the characteristic parameters of austenite stability, i.e., the

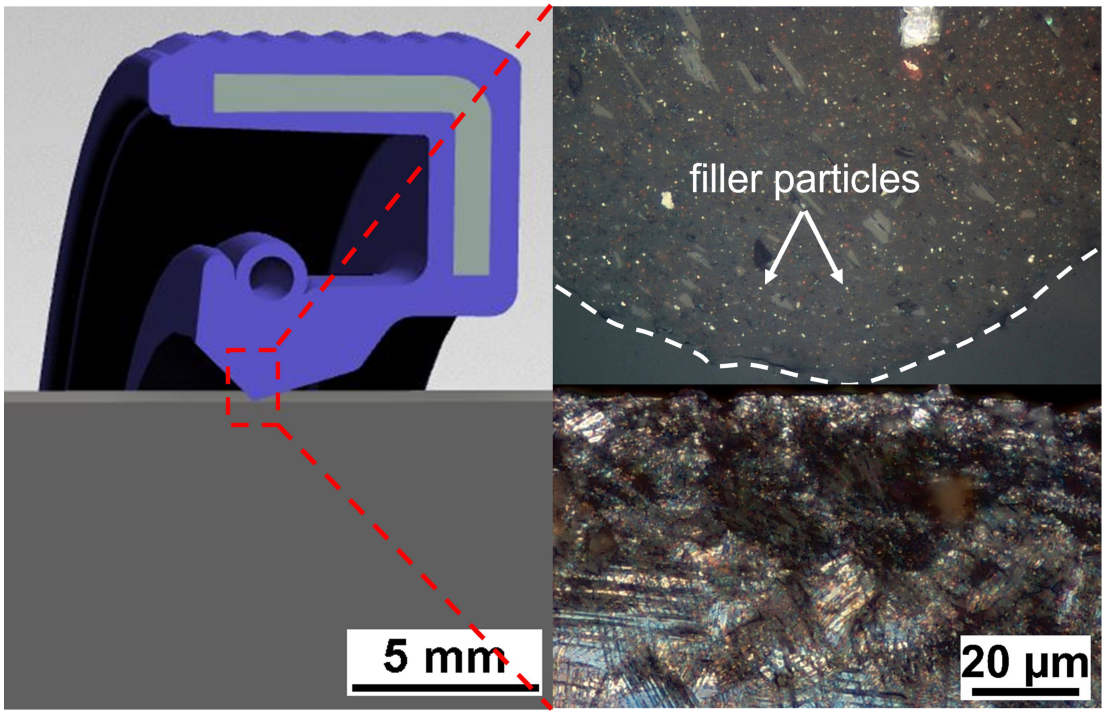


**FIGURE 1** Schematic illustration of the shaft wear process (cross section) and optical micrographs of cross-section of wear partner: sealing and shaft.

stacking fault energy, $M_{d30}$- and $M_s$-temperature, Table 1 [24, 26, 27]. The used equations are listed as followed:

$$M_{d30}\ \text{in}\ ^\circ\text{C} = 413 - 462 \cdot (C + N) - 9.2 \cdot Si - 8.1 \cdot Mn - 13.7 \cdot Cr - 9.5 \cdot Ni - 18.5 \cdot Mo \quad (1)$$

$$M_S\ \text{in}\ ^\circ\text{C} = 1578 - 41.7 \cdot Cr - 61.1 \cdot Ni - 33.3 \cdot Mn - 27.8 \cdot Si - 36.1 \cdot Mo - 1667 \cdot (C + N) \quad (2)$$

$$SFE\ \text{in mJ m}^{-2} = 2.2 + 1.9 \cdot Ni - 2.6 \cdot Si + 0.77 \cdot Mo + 0.5 \cdot Mn + 40 \cdot C - 0.016 \cdot Cr - 3.6 \cdot N \quad (3)$$

To ensure an entirely austenitic microstructure before subsequent cryogenic turning, the bulk material was annealed at 1050 °C for 35 min and then quenched in helium atmosphere to room temperature. Austenitic grains with annealing twins can be observed in the solution-annealed state, Figure 2. The average grain size in the initial state was 21 μm without considering the annealing twins.

## 4 | EXPERIMENTAL SETUP AND APPROACH

### 4.1 | Cryogenic turning process of metastable austenite

#### 4.1.1 | Single step turning process of metastable austenite

According to the previous study, the feed rate and the tool properties were varied to adjust the thermomechanical load in a targeted manner and thus improve the resulting surface morphology [28]. The increase of the feed rate, as well as the cutting-edge radius led to a higher passive force and therefore favored the deformation-induced martensite formation. However, these adjustments also led to an increase in surface roughness due to process kinematics and ploughing effects [29, 30].

For radial shaft seal counterfaces, it has been shown that a feed rate of $f = 0.15$ mm/rev and a corner radius of $r_\varepsilon = 1.6$ mm is ideal, because the surfaces generated with this feed rate showed reduced friction and wear compared to surfaces with lower feed rate while remaining leak tight [1]. The shaft wear for such surfaces was significantly reduced compared to case-hardened and infeed ground surfaces. Additionally, a further increase of deformation-induced martensite in the contact area during the test time due to the tribological processes could be determined. However, the influence of the amount and distribution of subsurface α'-martensite on wear resistance was not investigated in the above-mentioned work.

#### 4.1.2 | Cryogenic two-step turning of shaft counterfaces

Based on the study of the single step turning strategy, the cryogenic two-step turning process was developed, which has been proved to be an effective way of counteracting the conflict of objectives between attainable surface roughness and surface layer hardening. The aim of the first process step was to produce as much martensite as possible in the workpiece subsurface. For the second process step, the generated surface topography should be as favorable as possible, while the deformation-induced martensite produced from the first process step was to be kept in the subsurface. In previous investigations, which aimed mainly at maximizing the martensite content

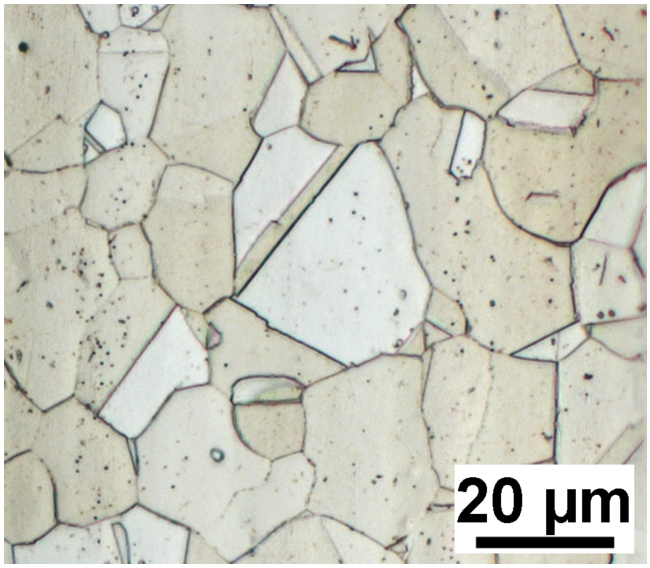


**FIGURE 2** Optical micrograph of the solution annealed AISI 347 specimen with purely austenitic microstructure.

**TABLE 1** Chemical composition in wt% of the investigated shaft material.

| C | N | Cr | Ni | Nb | Mn | Si | Mo | Fe | $M_{d30}$ | $M_s$ | SFE |
|---|---|---|---|---|---|---|---|---|---|---|---|
| | | | | [wt%] | | | | | [°C] | | [mJ/m²] |
| 0.02 | 0.02 | 19.29 | 9.25 | 0.41 | 1.55 | 0.63 | 0.19 | rest | 20.5 | −207.2 | 23.5 |

while maintaining a low surface roughness, a small feed rate of $f = 0.05$ mm/rev was used for the second step [28].

In this paper, the two-step turning process was adapted so that the resulting surface topography is optimally suited for the tribological system of radial shaft seal counterfaces. Two turning steps were performed quickly one after the other without changing tools. Thus, in the second process step no supply of coolant was necessary because the workpiece was still being strongly cooled by the precooling and the cooling from the first process step. Inserts made of uncoated carbide (89% tungsten carbide, 10% cobalt, 1% chromium; medium grain size: 0.42 μm) with the macro geometry DNMA150416 were used. A symmetrical rounding (form factor $k = 1$) with a medium sized cutting-edge radius of $r_\beta = 32$ μm was selected as microgeometry, which proved to be suitable for both process steps.

The carbon dioxide solid gas mixture was supplied at approx. −78 °C via two external nozzles. According to previous experiments, one nozzle supplied the coolant from the flank face and the other from the rake face direction [1, 28]. To improve the turning process in terms of economic and ecological aspects, the second turning step was carried out without cooling supply. The total consumption of carbon dioxide per workpiece is furthermore 1% lower compared to the conventional cryogenic turning process despite pre-cooling [1].

The cutting parameters used for the two-step turning process in this study are listed, Table 2. A high feed rate of $f = 0.65$ mm/rev was used in the first process step to achieve high passive forces und thus, promote the martensitic phase transformation. However, this feed rate is lower compared to the first process step of the two-step turning process used in previous investigations, because in this way the martensite distribution in the workpiece surface layer is more homogeneous in the feed direction [29]. A low cutting speed of $v_c = 30$ m/min was chosen to keep the temperatures in the workpiece surface layer as low as possible.

The beneficial thermomechanical load, which was adjusted in the first process step, led to a high content of martensite in the subsurface layer with increased hardness. Because of the high feed rate, the topography showed pronounced roughness peaks with a height of approx. 20 μm after the first process step. These roughness peaks were then removed in the second process step. The depth of cut was chosen very small to remove as little of the martensitic surface layer as possible. The depth of cut varied in the second process step due to the pronounced roughness peaks; it was $a_{p2,max} = 60$ μm at the roughness peaks and $a_{p2,min} = 40$ μm in the valleys between the roughness peaks. A cutting speed of $v_c = 100$ m/min together with the selected cutting-edge geometry and the low depth of cut led to a high surface quality. The choice of the cutting corner radius of $r_\varepsilon = 1.6$ mm in combination with the feed rate of $f = 0.15$ mm/rev led to an ideal surface topography for the tribological system of radial shaft seal counterfaces.

## 4.2 | Functional investigation of the shaft surface in a sealing system

In order to determine the wear resistance of the turned surfaces as counterfaces in the sealing contact with a radial shaft seal, endurance wear tests were performed on the two-step turned shafts. A 12-shaft test bench was used [16, 31]. The oil sump temperature was set to 70 °C, with a constant rotational velocity of 2,250 $min^{-1}$. The test duration of 590 h equals a sliding distance of 20,000 km. Flouroelastomeric radial shaft seals of the type BAUM 5X7 fabricated by Freudenberg & Co. KG were used in combination with non-additived synthetic polyalphaolefin oil (SAE grade: 0 W20). All test cells were filled up to the center of the horizontal shafts. A summary of the experimental configurations is listed, Table 3. A detailed description of the test bench can be found in a previous study [31].

Before and after the endurance wear test, the surface of all shafts and sealing edges was measured using a confocal microscope μSurf explorer (NanoFocus, Germany) and evaluated using MountainsMap and Matlab to determine the wear on shafts and seals. Furthermore, the radial force and contact area of the seals were measured to ensure an equal contact pressure for all experiments. Additionally, the geometry of the sealing edge was measured using a MicroCAD 3D microscope (LMI Technologies, Canada). After the test, those

**TABLE 2** Cutting parameters and coolant mass flow in the two-step turning process.

| | Feed rate f [mm/rev] | Cutting speed $v_c$ [m/min] | Depth of cut $a_p$ [mm] | Coolant-massflow $\dot{m}_{CO2}$ [kg/min] |
|---|---|---|---|---|
| Precooling | 0.2 | 30 | – | 3.5 |
| First process step | 0.65 | 30 | 0.15 | 3.5 |
| Second process step | 0.15 | 100 | 0.04–0.06 | – |

**TABLE 3** Configuration of the wear experiments in the sealing system.

| Endurance wear test | |
|---|---|
| Inner seal diameter [mm] | 80 |
| Seal material | Flouroelastomer (75 FKM 585) |
| Oil | Polyalphaolefin, SAE grade:0 W-20 |
| Rotational velocity [$min^{-1}$] | 2,250 |
| Oil sump temperature [°C] | 70 |
| Total sliding time [h] | 590 |
| Total sliding distance [km] | 20,000 |

measurements were repeated and the change in radial force and contact width as well as the wear on the shaft surface and the sealing edge was determined by comparing the new and worn condition.

## 4.3 | Investigation of the microstructural properties

In order to reveal the relationship between the manufacturing parameters and resulting wear behavior, a series of microstructural characterizations were carried out, including magnetic measurement, x-ray diffraction characterization as well as metallographic observation.

### 4.3.1 | Magnetic measurement

Based on the different magnetic properties of the initial γ-austenite and deformation-induced α'-martensite, Feritscope® measurements can be applied to evaluate the phase fraction of ferromagnetic contents in the surface-near regime up to a depth of 3 mm. Since the Feritscope® is usually used to evaluate the volume fraction of δ-ferrite in austenitic stainless weldments, the volume fraction of deformation-induced α'-martensite should be modified with a calibration factor $c = 1.71$ [32]. The sample surface was measured at four positions in the circumferential direction using Feritscope® FMP30 (Helmut Fischer Ltd., Germany). Three measurements were performed at each position. However, ε-martensite cannot be distinguished from the γ-austenite due to the similar paramagnetic properties.

### 4.3.2 | X-ray phase analysis

Comprehensive phase analyses of the processed sample surfaces were achieved using x-ray diffraction technique. The x-ray diffraction data was collected on diffractometers Empyrean and MRD Pro (both Malvern Panalytical Ltd., Netherlands). A spot size of 1.5 mm×1.5 mm was used at 40 kV and 40 mA with Copper-$K_{\alpha 1}$ radiation. For the phase fraction determination, the data was collected over the range $40\,^\circ < 2\theta < 100\,^\circ$ with a scanning speed of 0.005 °/s. The data was evaluated using the XRD-analysis software HighScore Plus (Malvern Panalytical Ltd., Netherlands) for the quantitative phase analysis based on the Rietveld-refinement method [33]. Besides, representative samples of both turning strategies were additionally electrolytical polished at 25 V for ~30 s using an etching device Lectropol-5 with electrolyte A2 (Struers, Denmark). The removed layer depth was measured with a high-resolution indicator (Mitutoyo, Japan) after each polishing step. Combined with the x-ray analyses, the phase distribution gradient in the surface-near regime can be determined.

### 4.3.3 | Metallographic observation

After turning with each strategy, a small part of the shaft with a length of around 25 mm was cut perpendicular to the circumferential direction. The samples were metallographically ground and carefully mechanical polished in order to avoid preparation-induced formation of martensitic phases. The samples were color-etched with Beraha-II reagent for metallographic observation.

### 4.3.4 | Focused ion beam (FIB) analysis

Considering the possible presence of nanocrystalline surface layers, focused ion beam analysis was carried out on representative samples manufactured with both turning strategies. Cross-sectional micrographs were deposited with platinum to ensure a flat surface without any edge-rounding and then cut with gallium primary ion beam at 30 kV. The focused ion beam analyses as well as scanning electron microscopy (SEM) investigations were conducted with a GAIA3 electron microscope (Tescan, Czech Republic).

## 5 | RESULTS

Six shafts were manufactured using the two-step turning process described in section 4.1.2. The surface profile was evaluated using MountainsMap, Figure 3. Some characteristic surface roughness parameters e.g., maximum height (*Sz*), arithmetical mean height (*Sa*) and root mean square height (*Sq*) are listed, Table 4. Except for shaft 4, where *Sz* is slightly above the

**TABLE 4** Evaluation of the areal surface characteristics of the turned shafts.

| Shaft | *Sz* [µm] | *Sa* [µm] | *Sq* [µm] |
|---|---|---|---|
| 1 | 3.53 | 0.34 | 0.41 |
| 2 | 3.54 | 0.63 | 0.73 |
| 3 | 3.59 | 0.57 | 0.67 |
| 4 | 4.28 | 0.45 | 0.55 |
| 5 | 3.42 | 0.58 | 0.68 |
| 6 | 3.42 | 0.61 | 0.71 |

recommendation for hard turned surface of 1 µm–4 µm, the values of *Sz* and *Sa* lie within the range proposed by the seal manufacturer for hard turned surfaces [17].

## 5.1 | Microstructural characterization of cryogenic turned samples

The microstructure of cross-sections of both cryogenic turned samples were investigated by optical and focused ion beam micrographs. After color-etching with the Beraha-II reagent, block and lath α'-martensite turned into dark blue or even black [23, 25], Figure 4a, b. Compared to the single step turning process, the two-step turning

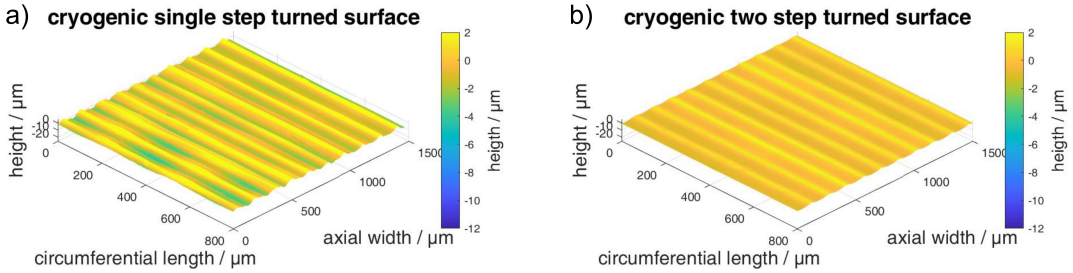


**FIGURE 3** Surface profile of a) cryogenic single step turned specimen and b) cryogenic two-step turned specimen.

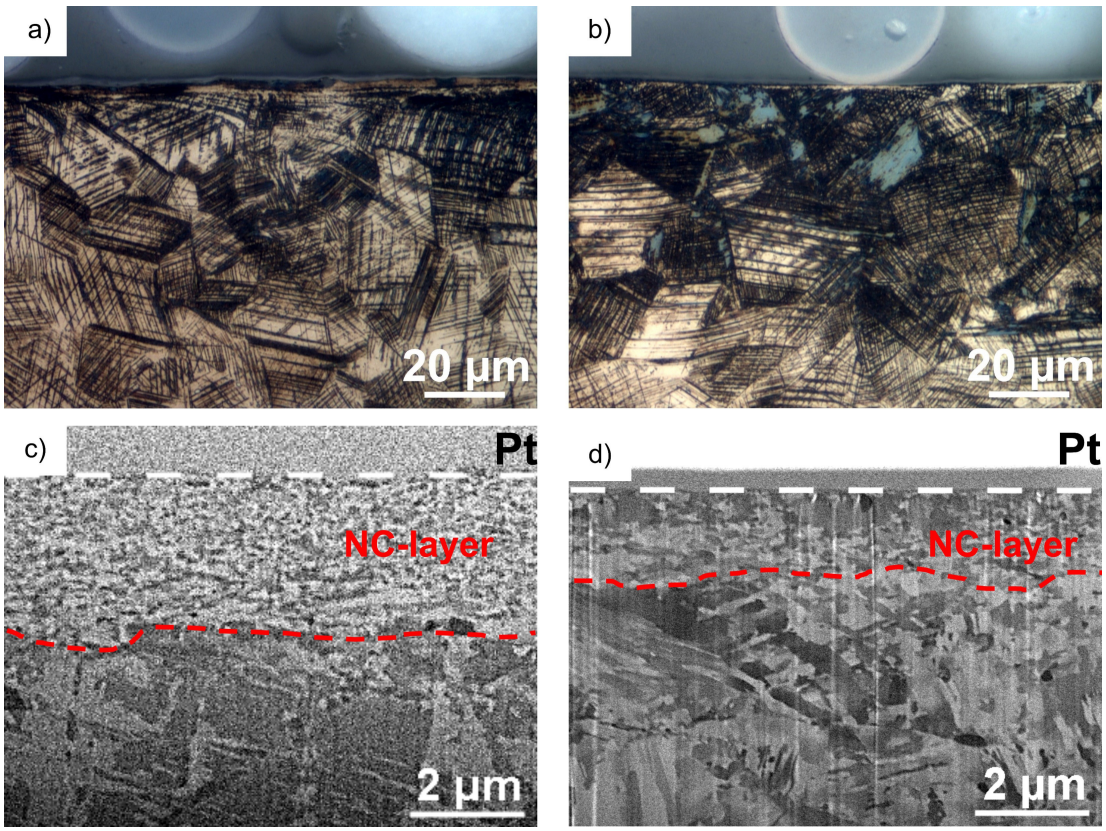


**FIGURE 4** Optical microscopy and focused ion beam image of single step turned shaft (a, c) and two-step turned shaft (b, d) in the surface-near regime.

strategy led to a higher absolute martensite content as well as higher transformation depth, which can be explained by the significantly higher mechanical loadings during the turning process. A thin brighter layer with the thickness of several micrometers can be observed after the two-step turning process, which indicates less deformation induced α'-martensite directly on the turned surface, Figure 4b. The higher working temperature due to the absence of coolant during the second process step clearly prohibited the local phase transformation in the surface near regime.

The focused ion beam analysis showed that nanocrystalline layers can be observed on both turned samples. Regarding the higher degree of deformation in the end manufacturing step, the single step turned sample showed a thicker nanocrystalline (NC) surface layer with a thickness of around 3 µm, while the layer thickness of the two-step turned sample was only about 1.5 µm, Figure 4c, d.

## 5.2 | Wear test

During the endurance test, a thermal overload occurred on shaft 5 due to a faulty temperature control. This led to an overall leakage of 4.695 g of oil during the test due to thermal damage of the seal. All other shafts showed no measurable leakage at all. Therefore, the results of the endurance wear test on shaft 5 were disregarded. Surfaces 1, 3, and 6 show a clear wear track while surfaces 2 and 4 show no measurable wear, Figure 5. Additionally, a pile up of material around the wear track was found on shaft 3 and 6. The pile up could not be removed by a cleaning process using propanone (acetone). It is to be assumed that the pile up consists of charred oil (due to high temperatures in the sealing contact). Similar results have been found in previous investigations [20].

Compared to the cryogenic single step turned samples, the average planimetric wear of two-step turned samples is slightly higher, Figure 6. However, it is still significantly lower than the wear of the ground carburized AISI 5115 state of the art shafts, Figure 7.

## 5.3 | Microstructural characterization of worn samples

Due to the low wear depth ($d_{wear} \leq 10$ µm), the microstructural changes can hardly be identified on the optical metallographs, Figure 8a, b. When compared to the focused ion beam images of cryogenic turned surfaces in Figure 4c, d, the nanocrystalline layer remained distinguishable on the single step turned shaft even after wear, Figure 8c. Conversely, beneath the wear track of all two-step turned shafts (except for shaft 5), only coarse grains were observable, Figure 8d.

## 5.4 | XRD phase analysis

Considering the low penetration depth of x-ray of 8 µm at an incident angle $\theta = 50°$, the x-ray phase analysis provides adequate information about the local distribution of phase contents near the surface of the worn zone. From the surface to the subsurface, both samples showed a slight increase in the deformation-induced α'-

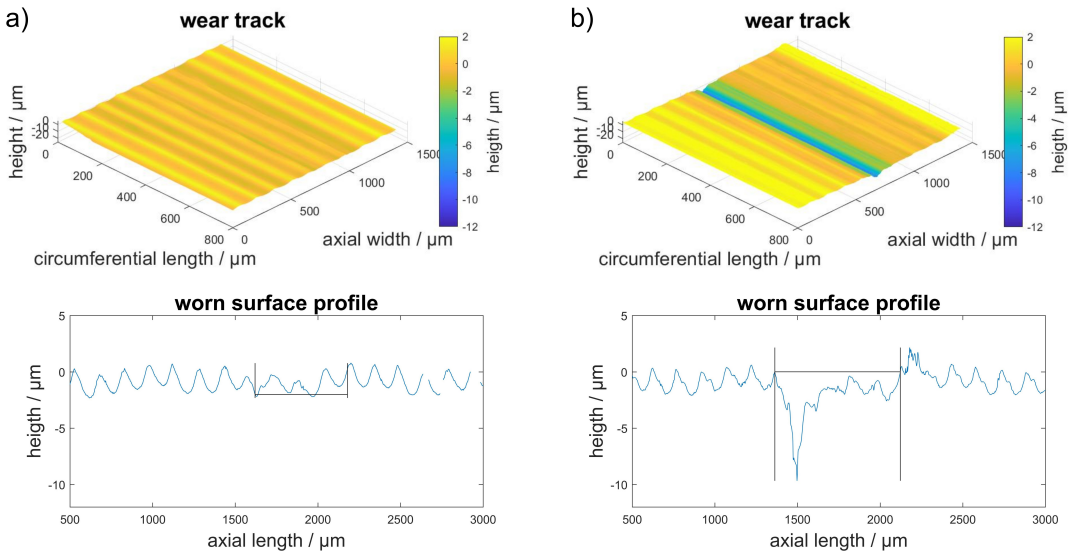


**FIGURE 5** Confocal measurements of the wear track and wear profiles of exemplary two-step turned shafts with no measurable wear (shaft 2, (a)) and clear wear track (shaft 3, (b)).

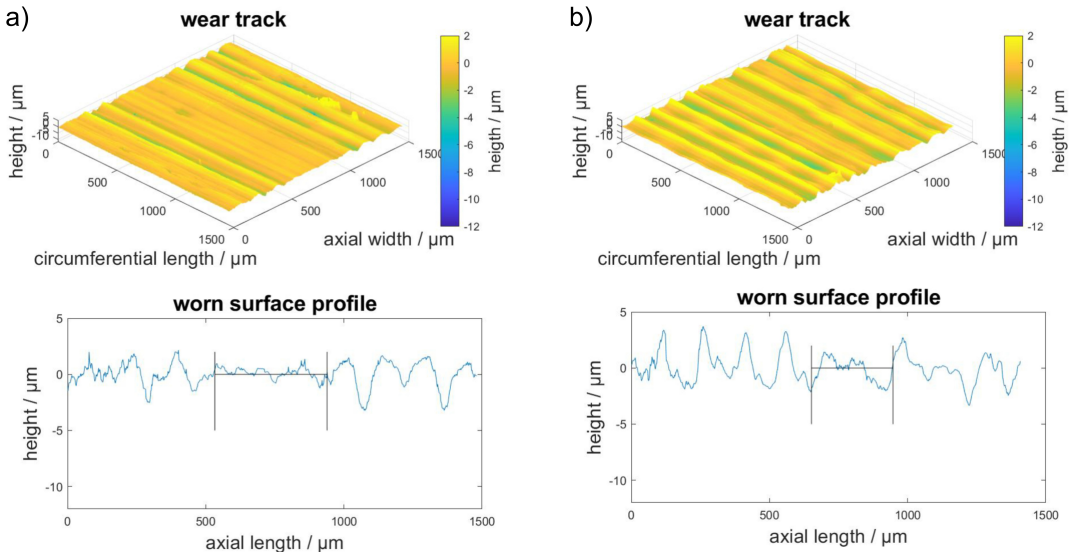


**FIGURE 6** Confocal measurements of the wear track and wear profiles of cryogenic single step turned shaft (a) according to [20] and two-step turned shaft (shaft 6, (b)).

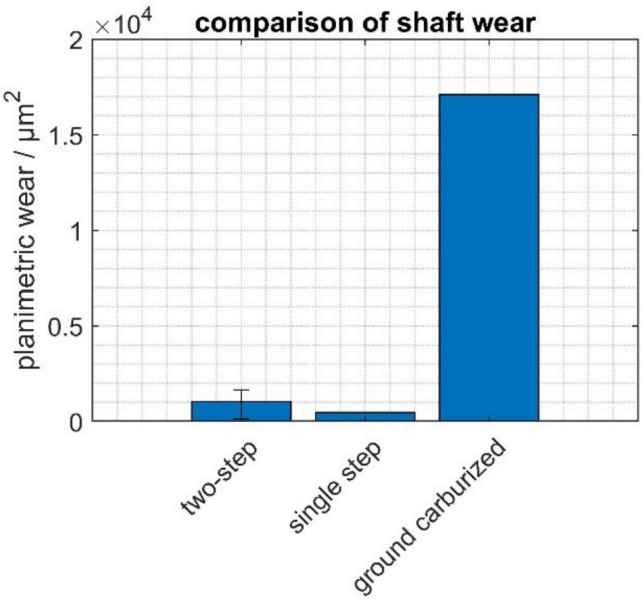


**FIGURE 7** Comparison of planimetric shaft wear of the shafts turned in a two-step turning process, the cryogenic single step turning process and a state of the art ground carburized shaft [1].

martensite phase fraction. The volume fraction of α'-martensite reached its maximum value at around 10–20 µm. Afterwards, the volume fraction of α'-martensite began to decrease gradually, Figure 9. Besides, ε-martensite can be detected at the same point. With gradually increasing distance from the surface, the maximum volume fraction of ε-martensite appeared at a depth of around 50 µm and remained relatively constant along the following measurements. Despite the similar depth distribution and maximum value, less γ-austenite can be detected beyond the worn range, which correlates very well with the Feritscope® measurements.

Only 20 vol% α'-martensite was induced directly on the sample surface after the two-step turning strategy, while 28 vol% were found at the surface of the single step turned sample. A possible explanation may be the higher thermal loads of the second process step of the two-step turning strategy owing to the higher feed rate as well as the absence of coolant. The precedent volume content of deformation-induced α'-martensite on the single step turned seal shaft can be observed until a depth of around 10 µm. Since the maximum worn depth among all turned shafts investigated in this study was only 8 µm, the better wear resistance of the single step turned shaft could be attributed its higher deformation-induced martensite fraction.

## 5.5 | Magnetic characterization

According to the Feritscope® measurements, a higher ferromagnetic fraction can be detected on the two-step turned shaft compared to the cryogenic single step turned sample. After the cryogenic single step turning, the ferromagnetic α'-martensite increased to around 3 vol%, while the two-step turned sample has reached around twice as much, Figure 10b. Despite the same cutting depth, the higher feed rate in the first process step of the two-step turning strategy led to a higher total phase transformation due to the higher mechanical loading [29]. With help of polynomial curve fitting and mathematical integral calculations, a similar conclusion can be drawn from the x-ray phase gradient measurements, Figure 10a, b.

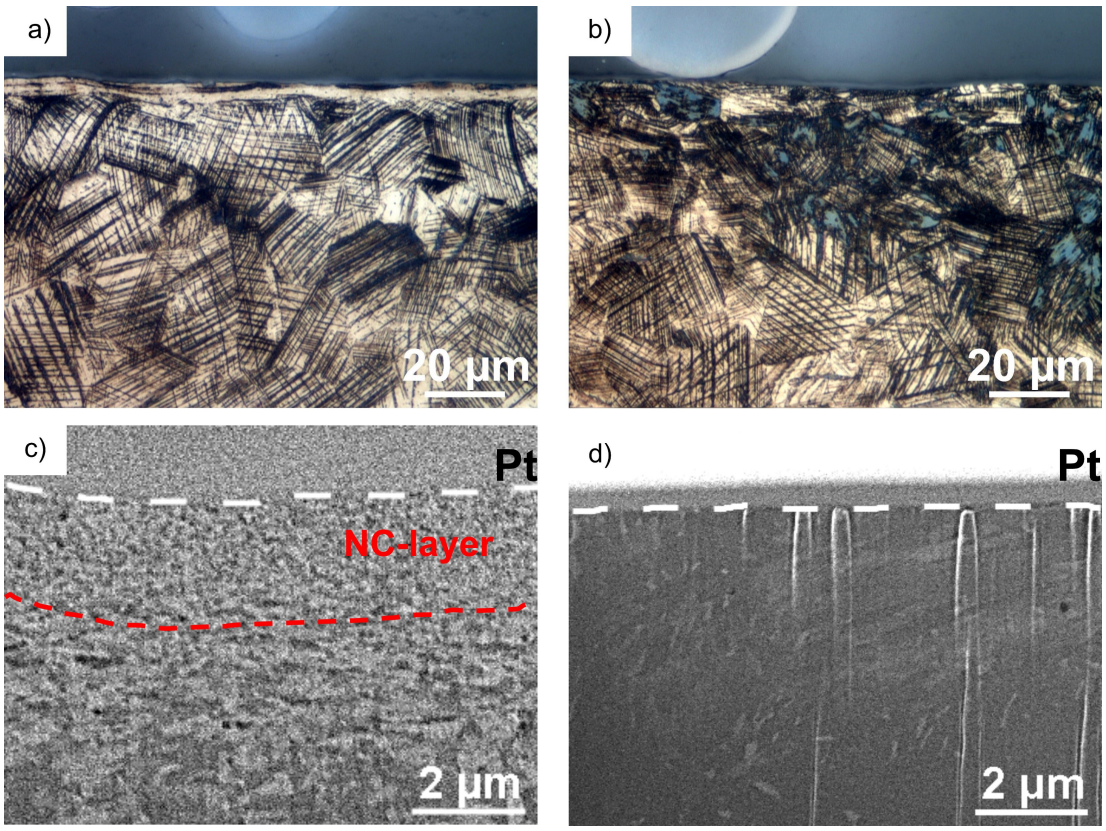


**FIGURE 8** Optical microscopy and focused ion beam image of a worn single step turned (a, c) and two-step turned (b, d) sample.

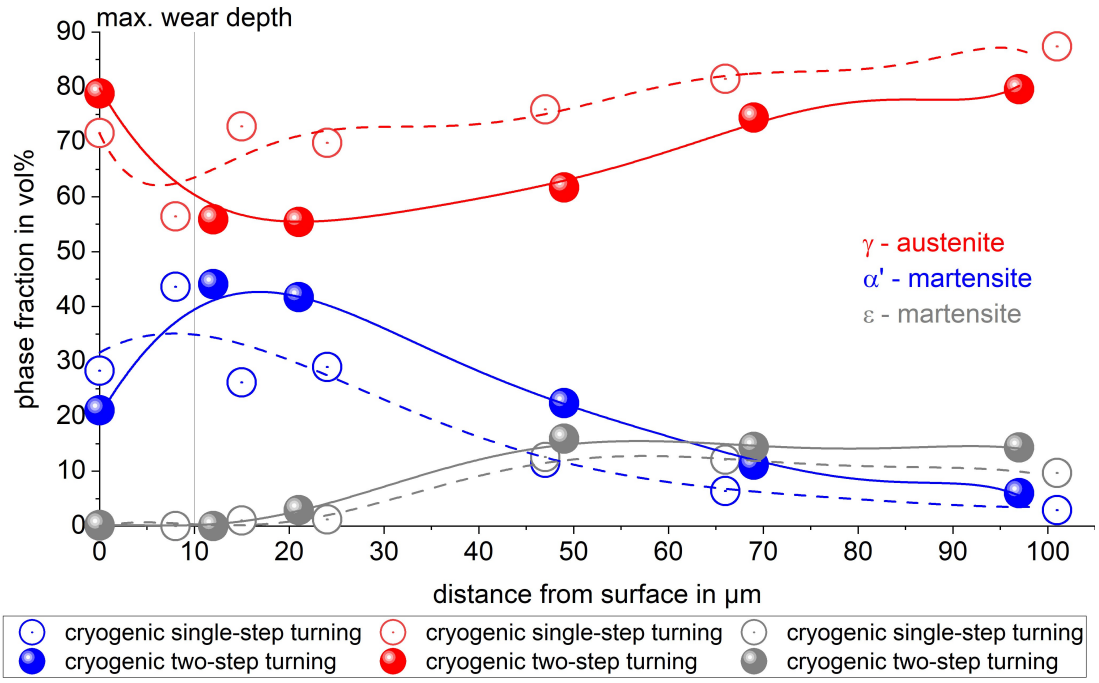


**FIGURE 9** Phase distribution in the near surface regime of samples produced with both turning strategies.

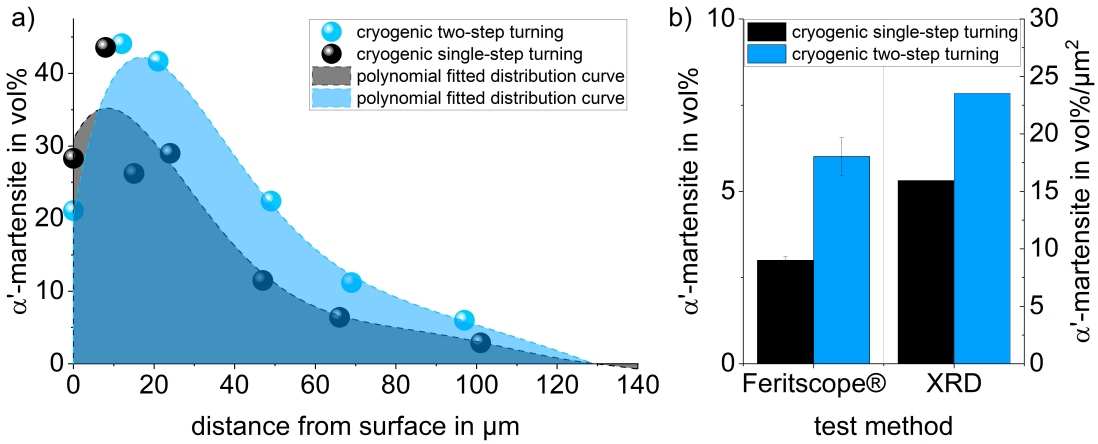


**FIGURE 10** a) polynominal fitting of the α'-martensite volume fraction according to the x-ray phase analysis b) comparison of the α'-martensite volume fraction between Feritscope® measurements and integral of XRD analysis.

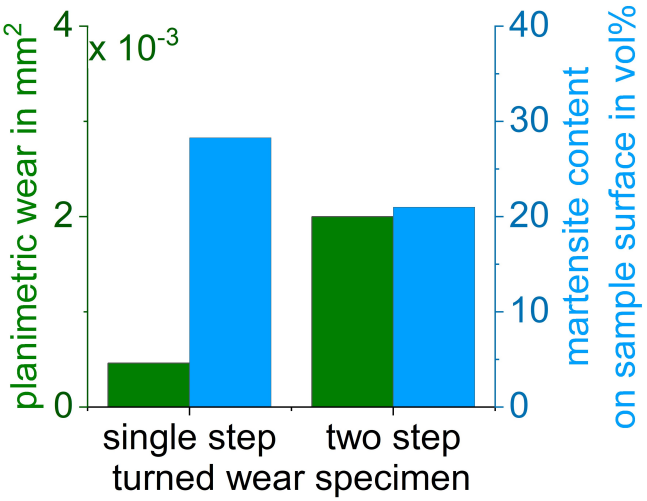


**FIGURE 11** Comparison of planimetric shaft wear and surface martensite fraction of the shafts turned in a two-step turning process and single step turning process [1].

Regarding the above-mentioned experimental results, various characterization methods may lead to different conclusions. Generally, the higher total martensitic phase transformation can be confirmed by both magnetic and x-ray measurements. However, the locally inhomogeneous distribution of the deformation-induced α'-martensite played the key role for the wear test, since the maximum wear depth is only up to 10 µm. In this case, the x-ray analysis is more representative and should be considered as the appropriate method to characterize the wear zone, despite the fact that magnetic measurement is much more convenient and cost-effective.

The superior wear resistance of the cryogenic single step turned sample can be well explained by the local predominance of martensitic phase transformation on the surface, Figure 11. Moreover, the thicker nanocrystalline surface layer (see section 5.5) on the single step turned sample can also play a positive role on the wear behavior [34].

## 6 | SUMMARY

Based on the previous study of a cryogenic two-step turning strategy for metastable austenitic stainless steel AISI 347, a similar application for shaft counterfaces was investigated.

Compared to the cryogenic single step turned sample, the two-step turning process can generate more deformation-induced α'-martensite in the sample subsurface up to 150 µm, while guaranteeing a good surface morphology via the second turning step. However, the local microstructure in the first 10 µm played a more important role under the specific wear conditions investigated. Benefiting from the local predominance of deformation-induced α'-martensite and nanocrystalline surface layer, the single step turned shaft showed a better wear resistance than the two-step process despite less integral phase transformation.

The results demonstrate the influence of manufacturing processes on the surface morphology, and subsequently the wear behavior. In terms of the microstructure characterization, apparently the locally resolved x-ray diffraction measurements directly on the surface were more suitable to characterize component surfaces for the specific tribological application in a sealing system compared to integral magnetic measurements. Furthermore, this research pointed out the importance of local adjustment of surface properties by the manufacturing process.

## ACKNOWLEDGEMENT

Funded by the Deutsche Forschungsgemeinschaft (DFG, German Research Foundation) – Project-ID 172116086 – SFB 926. Open Access funding enabled and organized by Projekt DEAL.

## CONFLICT OF INTEREST STATEMENT

The authors declare no conflicts of interest.

## ORCID

*T. Zhu* http://orcid.org/0000-0002-0320-5787

## REFERENCES

1. D. Frölich, B. Magyar, B. Sauer, P. Mayer, B. Kirsch, J. C. Aurich, R. Skorupski, M. Smaga, T. Beck, D. Eifler, *Wear* **2015**, *328–329*, 123.
2. S. Jung, *Ph.D. Thesis*, University of Stuttgart, Germany **2012**.
3. M. Smaga, R. Skorupski, P. Mayer, B. Kirsch, J. C. Aurich, I. Raid, J. Seewig, J. Man, D. Eifler, T. Beck, *Procedia Structural Integrity* **2017**, *5*, 989.
4. M. J. Sohrabi, M. Naghizadeh, H. Mirzadeh, *Archiv.Civ.Mech.Eng* **2020**, *20*.
5. I. S. Jawahir, H. Attia, D. Biermann, J. Duflou, F. Klocke, D. Meyer, S. T. Newman, F. Pusavec, M. Putz, J. Rech, V. Schulze, D. Umbrello, *CIRP Annals* **2016**, *65*, 713.
6. I. Nikitin, B. Scholtes, *HTM - J. Heat Treat. Mater.* **2012**, *67*, 188.
7. F. Ambrosy, F. Zanger, V. Schulze, I. S. Jawahir, *Procedia CIRP* **2014**, *13*, 169.
8. G. Gershteyn, N. Shevchenko, M. Diekamp, A. Brosius, M. Schaper, F.-W. Bach, *Mat.-wiss. u. Werkstofftech.* **2012**, *43*, 262.
9. J. C. Aurich, P. Mayer, B. Kirsch, D. Eifler, M. Smaga, R. Skorupski, *CIRP Annals* **2014**, *63*, 65.
10. D. Frölich, B. Magyar, B. Sauer, *Wear* **2014**, *311*, 71.
11. A. Schubert, R. Zhang, P. Steinert, *Procedia CIRP* **2013**, *7*, 294.
12. A. Schubert, P. Steinert, M. Kirbach, R. Zhang, H. Zeidler, *ICMC 2014 proceedings* **2014**.
13. R. Zhang, A. Schubert, H. Zeidler, *Zeitschrift für wirtschaftlichen Fabrikbetrieb* **2014**, *109*, 889.
14. P. Steinert, A. Nestler, J. Kühn, A. Schubert, *Proceedings COMA'16*, South Africa **2016**.
15. T. Leichner, V. Franke, B. Sauer, J. C. Aurich, *Prod. Eng. Res. Devel.* **2011**, *5*, 531.
16. S. Thielen, B. Magyar, B. Sauer, F. Schneider, P. Mayer, B. Kirsch, R. Müller, E.v. Harbou, J. C. Aurich, *Tribology International* **2018**, *118*, 442.
17. Freudenberg Sealing Technologies GmbH & Co. KG, *Technisches Handbuch-Ausgabe 1* **2015**.
18. R. Flitney, *Seals and Sealing Handbook*, Butterworth-Heinemann **2014**.
19. L. Horve, *SAE Transactions* **1991**, *100*, 620.
20. C. Burkhart, S. Emrich, M. Kopnarski, B. Sauer, *Wear* **2020**, *460–461*, 203419.
21. C. Burkhart, Heier, M., Merz, R., J. Lösch, C. Wagner, S. Thielen, B. Sauer, M. Kopnarski, H. Hasse, presented at *62nd Tribology Conference*, Göttingen, **2021**.
22. G. B. Olson, M. Cohen, *Metall and Mat Trans A* **1976**, *7*, 1897.
23. M. Smaga, A. Boemke, T. Daniel, M. W. Klein, *MATEC Web Conf.* **2018**, *165*, 4010.
24. M. Naghizadeh, H. Mirzadeh, *Metall Mater Trans A* **2018**, *49*, 2248.
25. M. Naghizadeh, H. Mirzadeh, *Metall Mater Trans A* **2016**, *47*, 4210.
26. T. ANGEL, *J. Iron Steel Inst.* **1954**, *177*, 165.
27. G. Meric de Bellefon, J. C. van Duysen, K. Sridharan, *Journal of Nuclear Materials* **2017**, *492*, 227.
28. H. Hotz, B. Kirsch, S. Becker, E. von Harbou, R. Müller, J. C. Aurich, *Procedia CIRP* **2018**, *71*, 160.
29. H. Hotz, M. Smaga, B. Kirsch, T. Zhu, T. Beck, J. C. Aurich, *Procedia CIRP* **2020**, *87*, 35.
30. H. Hotz, B. Kirsch, J. C. Aurich, *J Intell Manuf* **2021**, *32*, 877.
31. S. Thielen, P. Breuninger, H. Hotz, C. Burkhart, T. Schollmayer, B. Sauer, S. Antonyuk, B. Kirsch, J. C. Aurich, *Tribology International* **2021**, *155*, 106764.
32. J. Talonen, H. Hänninen, P. Nenonen, G. Pape, *Metall and Mat Trans A* **2005**, *36*, 421.
33. R. A. Young, *The rietveld method*, Oxford University Press, Oxford, **1993**.
34. M. Laleh, F. Kargar, M. Velashjerdi, *J. of Materi Eng and Perform* **2013**, *22*, 1304.

**How to cite this article:** T. Zhu, M. Smaga, S. Thielen, H. Hotz, B. Kirsch, J. C. Aurich, B. Sauer, O. Koch, T. Beck, *Materialwiss. Werkstofftech.* **2024**, *55*, e202300007. https://doi.org/10.1002/mawe.202300007